ON THE POSSIBILITY OF MATHEMATICAL MODELING OF SEPARATED FLOWS BY SOLVING THE EULER EQUATIONS

ICAS-94-5.7.4

V.V. Vyshinsky and S. A. Kravchenko
Central Aerohydrodynamic Institute (TsAGI)
Moscow, Russia

Abstract

Using as an example a rather complicated aerodynamical problem of computing flow around a two-body system (reentry vehicle-impermeable parachute), the possibility of modeling separated flows within the framework of a boundary-value problem for the unsteady Euler equations is investigated. Available data on force tests and flow visualization allow the numerical method to be effectively verified.

I. Introduction

In real flows of a compressible viscous gas there are the two main mechanisms of vorticity generation: viscous and entropic (in curved shocks). Essential features of the Euler equations are the rigorous modeling of vorticity transport in compressible gas flow and the absence of a viscous mechanism of vorticity generation.

In numerically solving a boundary-value problem for the Euler equations, the influence of physical viscosity can be taken into account with the help of special operators introduced into the computational algorithm, and the presence of artificial viscosity in the tensor form results in the appearance of non-physical diffusion and dissipation in the solution. This imposes certain requirements on specifying boundary conditions and computational grid generation to obtain satisfactory results for various bodies and flow regimes: the same value of numerical viscosity determined by a measure of grid resolution (the number of grid points) may turn out to be unacceptable for an attached flow around an airfoil and sufficient for computing flow over a bluff body.

The present work addresses the problem of external flow around a two-body configuration at $0.8 \le M_\infty \le 1.7$. The influence of computational grid topology and boundary condition statement associated with the problem on the accuracy and physical meaningfulness of solutions being obtained are investigated. The boundary-value problem on the accuracy and physical meaningfulness of solutions being obtained are investigated. The boundary-value problem being solved corresponds to modeling separated flow around the two-body configuration in a wind tunnel. But to what degree the natural phenomenon being investigated is modeled under aerodynamic test conditions in view of its unsteadiness and non-axisymmetry remains an open question.

II. Problem formulation and the discussion of the model employed

The substantially unsteady three-dimensional problem of deceleration (from freestream Mach number $M_\infty = 1.7$ to $M_\infty = 0.7$) of a reentry vehicle-parachute configuration is considered. For constructing the mathematical model several assumptions are made.

The problem is treated as steady, using an inertial body-fixed coordinate system with freestream being steady and uniform. The permeability of parachute material is ignored (this question is investigated in[1]) as well as the dynamics of parachute deployment and variations of shape of parachute canopy according to the pressure difference across it (see, e.g.[2]). The influence of shroud lines, parachute longitudinal and lateral oscillations and spinning due to a large number of degrees of freedom is neglected, but the unsteadiness associated with the formation of separated flow structures and solution oscillations at M_∞ = const in the case of the stationary rigid parachute are taken into consideration. Such a statement allows experimental results to be

Copyright © 1994 by ICAS and AIAA. All rights reserved.

used for verifying solutions obtained. In the present case, the effects of wind tunnel walls and gas viscosity are not taken into account in numerical modeling.

The flow is assumed to be axisymmetric, which excludes the canopy's non-axisymmetry and non-axisymmetrical perforations in it.

Thus, the separated flow around the combination of the two rigid bodies (Fig. 1) is computed using the unsteady Euler equations:

$$\frac{\partial \rho}{\partial t} + \nabla\{\rho\cdot\vec{V}\} = 0 ,$$

$$\frac{\partial \rho\vec{V}}{\partial t} + \nabla\{\rho\,\vec{V}\cdot\vec{V}\} = -\nabla p,$$

$$\frac{\partial \rho E}{\partial t} + \nabla\{(\rho E+p)\vec{V}\} = 0 ,$$

where ρ is the density, p is the pressure, $E = e + V^2/2$, $e = p/\rho/(\kappa-1)$ for the ideal gas, κ is the ratio of specific heats. The tangency conditions on the surface $\partial\Omega$ of the reentry vehicle and on both sides of the surface $\partial\Omega_1$ of the parachute are

$$(\vec{V}, \vec{N})_{|\partial\Omega \cup \partial\Omega_1} = 0. \qquad (2)$$

The shape of the parachute surface $\partial\Omega_1$ is specified beforehand according to the shape of a rigid parachute for wind tunnel testing or, in the case of a soft parachute, using photographs taken during experiment.

At "left-hand infinity" the undisturbed free-stream flow conditions are specified:

$$\begin{aligned} p_{|x\to-\infty} &\to p_\infty , \\ \rho_{|x\to-\infty} &\to \rho_\infty , \\ \vec{V}_{|x\to-\infty} &\to \vec{i}\cdot V_\infty , \end{aligned} \qquad (3)$$

where $\vec{i}$ is the unit vector of the x-axis. Specified at "right-hand infinity" are zero derivatives in the direction of the normal $\vec{N}$ to the boundary of the computational domain:

$$\begin{aligned} \frac{\partial p}{\partial N}_{|x\to\infty} &\to 0, \\ \frac{\partial \rho}{\partial N}_{|x\to\infty} &\to 0, \\ \frac{\partial V}{\partial N}_{|x\to\infty} &\to 0. \end{aligned} \qquad (4)$$

The equations of motion are nondimensionlized using the freestream parameters $p_\infty, \rho_\infty, V_\infty$ and the canopy diameter D as characteristic values. By way of the integration of pressure distribution over the reentry vehicle surface and both sides of the parachute surfaces the force values are found which are divided by the dynamic pressure $q_\infty = \rho_\infty\cdot V_\infty^2/2$ and the characteristic areas ($\pi\cdot d^2/4$ for the reentry vehicle, where d

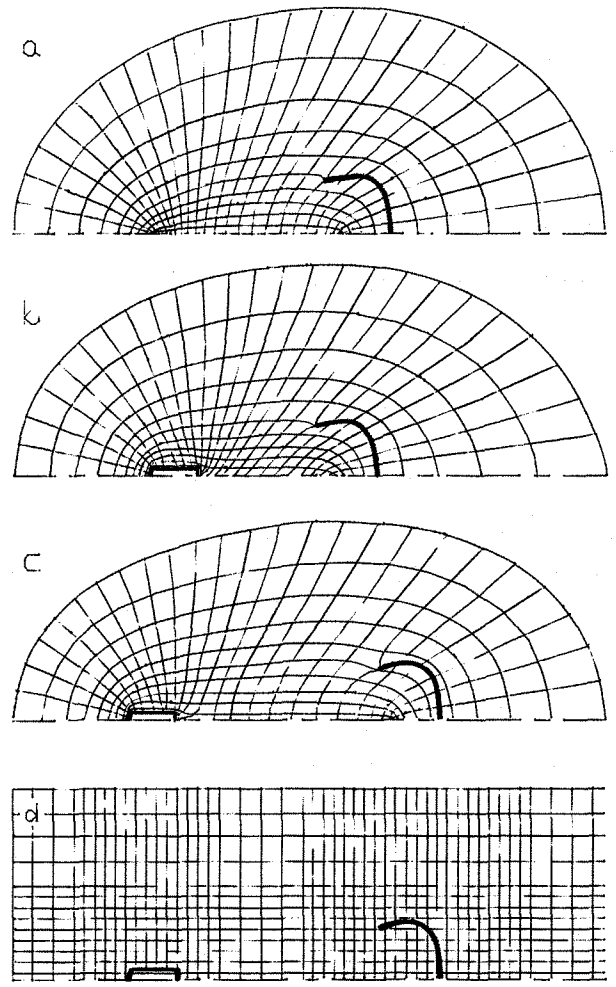

Figure 1. A schematic view of the three O-type (a,b,c) and H-type (d) grids, used in computation.

is the base diameter, and $\pi\cdot D^2/4$ for the parachute) to obtain the drag coefficients C_d and C_D. The base drag coefficient C_{d_b} for the reentry vehicle and C_{D_B} for the parachute are also determined, with integration carried out over the reentry-vehicle base in the first case and over the canopy external surface in the second case.

For solving the boundary-value problem the upwind difference scheme is used, stable without artificial dissipation. The integration with respect to time in the framework of the finite volume concept is performed using a single temporal metric for the space so that the time step size at a specified Courant number[3] is determined by the minimum volume of computational grid cell. Details of the computational method used and results of its verification for the case of isolated bodies may be found in[4] and[5]. Considered for all the computations are peculiarities of the solutions on the grids of two topologies: a curvilinear orthogonal O-type grid for which the body contour is one of the coordinate lines and an H-type grid, whose structure is similar to a Cartesian coordinate system.

III. A solution method for the boundary-value problem

Solving the problem on both grids is performed using an axisymmetrical approximation in a cylindrical coordinate system x, r, ϑ, with the x-axis being directed along the flow symmetry axis. The algorithm used performs computation for one longitudinal meridional section ϑ = const of the flow. A method of[4] employed herein is based on a finite-volume scheme with the first order accuracy in time and space[6]. The scheme has no artificial viscosity because the upwind difference method used is stable with no additional dissipative terms.

The presence of numerical (unavoidable) viscosity in a tensor form (see, for example,[6])

$$\mathbf{W} \sim \rho \cdot \begin{Vmatrix} u\cdot\Delta x \dfrac{\partial u}{\partial x} & v\cdot\Delta y \dfrac{\partial u}{\partial y} \\ u\cdot\Delta x \dfrac{\partial v}{\partial x} & v\cdot\Delta y \dfrac{\partial v}{\partial y} \end{Vmatrix}$$

leads to the fact that a differential approximation of the original set of the Euler equations is a system of "pseudo-Navier-Stokes" equations (see, for example,[7]) used in computing:

$$\frac{\partial \rho}{\partial t} + \nabla\{\rho\cdot\vec{V}\} = 0,$$

$$\frac{\partial \rho\vec{V}}{\partial t} + \nabla\{\rho\cdot\vec{V}\cdot\vec{V}\} = -\nabla(p\cdot\mathbf{I} + \mathbf{W}),$$

$$\frac{\partial \rho E}{\partial t} + \nabla\{(\rho E + p)\vec{V}\} = -\mathbf{W} : \nabla\vec{V},$$

where I is the unit matrix. Generally speaking, the boundary-value problem does not possess an unique solution, if a differential approximation to the boundary conditions on the body are the tangency conditions. In this case the uniqueness of the solution is established by the surface break between the conical and cylindrical parts of the reentry vehicle, the corner of its flat base, where in the small (in the case of an indefinite normal) the no-slip condition is modeled, and the sharp parachute leading edge (a Kutta-Joukowsky-type condition).

Artificial viscosity generates numerical diffusion which suppresses short waves in the solution and leads to widening any discontinuity (shock, mixing layer) by a value greater than mesh spacing. Long waves (by the way, the grid methods are basically a tool to study a long-wave approximation) are minimally affected by numerical diffusion, which permits solutions with shocks to be considered where (now due to numerical viscosity) the transformation of short-wave kinetic energy into thermal energy takes place. In similar fashion, the dissipation of short-wave energy occurs and vorticity is generated in the mixing layer demarcating the separated zone of circulating motion from the external flow.

As shown in[4-6] and[8], separated flow with zones of circulating motion may be successfully simulated in the framework of ideal gas concept by solving the unsteady Euler equations containing a vorticity transfer mechanism. In this case, along with a physical mechanism of vorticity generation in curved shocks with variable entropy along their fronts there is a non-physical vorticity generation mechanism due to numerical vorticity in the computational scheme. The numerical vorticity are caused by the approximation to the equations of motion and boundary conditi-

ons, especially when using a H-type grid, where the tangency condition (2) is specified on a stepped line representing the body surface and coinciding with the grid lines x_i= const, r_j=const, nearest to the surface. In so doing, at each corner point (i,j) of the stepped line $v|_{r=r_j} = 0$, $u|_{x=x_i} = 0$ the no-slip condition ($u_{ij} = v_{ij} = 0$) is modeled in the small; in the vicinity of each corner point a mixing zone occurs and an intensive vortex formation takes place.

With a sufficiently accurate solution approximation (high grid density) the size of the approximating line steps diminishes (the "angularity"of the approximating line and the vorticity generated by the angularity decrease and only the vorticity associated with the "true" surface breaks remains), the number of steps increases and the solution is stabilized in a pseudo-viscous way. For example, the influence of the stepped approximating line of reentry vehicle on the solution becomes negligibly small with grid refining in comparison with the effects of the cone-cylinder break and base corner.

The computation was performed on a comparatively coarse grid not always sufficient for obtaining a high levelof resolution in the vicinity of the reentry vehicle and parachute,and especially in the zone between them. The latter region is of great importance in investigating the so-called "aerodynamic reefing" of parachute.

In the present method particular attention was focused on the choice of grids[9] that makes it possible to account for the influence of the separated flow around the first body (reentry vehicle) on the flow about the second body (rigid parachute), the issue not considered in[1] and[2].

The boundary conditions at infinity (3),(4) for all the grids used are specified at the computational domain boundary, which, as distinct from[4], limits the freestream Mach number M_∞ below. Such an approach is traditional (see, for example,[6]). The question of the sufficiency of computational domain size for the transonic problems in the framework of the Euler equations is investigated in[10]. In particular,for the two-dimensional circulatory case a size of about 50 airfoil chords was found to be sufficient. For the noncirculatory three-dimensional case this size can be substantially diminished due to a more rapid attenuation of disturbances with increasing the distance from the body. In[4] the questions associated with the asymptotic behaviour of the solution at infinity are resolved as an external potential problem relative to the internal vortical do main using a well-established finite-difference method for the potential equation on the O-type grid with the mapping of the exterior domain relative to the zeroth streamline, which bounds the body and the closed separated zone behind it, into an open disk,and infinity into its center. This approach permits the computational domain boundary to be chosen correctly (on the order of 10 characteristic lengths for the problem) in formulating boundary conditions.

A schematic view of internal details of the three O-type grids used in computation is presented in Fig.1. All of them have 100 rays with 50 mesh points on each and the same topology near the computational domain boundary. At the external boundaries of the computational domain the coordinate lines ξ=const and η=const are orthogonal.

A distinctive feature of the first grid used for computation of the flow around the isolated parachute ($L \to \infty$, where L is the distance between the base of the reentry vehicle and the mouth section of the parachute) is the orthogonality of the coordinate lines on the axis of symmetry r = 0.

The single grid for computing the flow around the two-body configuration at a body-to-body distance of $\overline{L}$ = L/D=1 has non-orthogonal coordinate lines (skewed cells) in the axis of symmetry as opposed to the above grid. They are non-orthogonal on the reentry vehicle's surface as well, especially on its base and, as in the first case, on the parachute's surface and to the largest extent near the parachute's mouth section.

The third grid used for computig the flow around the two-body configuration at $\overline{L}$ = 1.75 has no above shortcomings:

it is orthogonal on the base as well as on the axis of symmetry.

Both the second and third grids are used to compute flow around the isolated reentry vehicle. In this case, the tangency conditions on the line modeling the parachute is removed. The size of the computational domain is approximately 20·L×10·L, where L is a characteristic scale of the problem.

Along with regular O-type grids, nonregular Cartesian orthogonal H-grids were used in a cylindrical coordinate system with the x-axis being the axis of symmetry of the flow (see Fig.1,d). The entire flowfield in this case is divided into two computational regions: for the reentry vehicle and for the parachute. In each region there are 6 blocks within which the grid spacing is constant (but different in the x- and r-directions). At the block interfaces the grid spacing along the common boundary is the same for two adjacent blocks. The total number of grid points for the two-body configuration is 2·50·50, and for the isolated reentry vehicle and parachute 50·50 and 50·60, respectively.

The method was implemented on a computer with a speed of 0.25 Mflops. The computation of 1000 time steps takes about one hour of computer time. Convergence analysis and investigation of accuracy of results are presented in [4] and [5].

IV. Computational results

As the first example of the computational results, Fig.2 shows flow about the isolated reentry vehicle - a cone-cylinder body with a cone angle of φ = 150°, a cone fineness ratio of $\lambda_n = L_n/d$ = 0.12 and a cylinder fineness ratio of $\lambda_c = L_c/d$ = 2.5, where L_n and L_c are the lengths of the conical and cylindrical parts of the reentry vehicle, respectively. The cylindrical portion ends with the flat base, at whose corner the no-slip condition is specified and the separation location is fixed naturally. In this case the separation occurs because of fluid particles' inertia and the presence of artificial viscosity which does not allow the tangency condition (2) to be imposed "immediately" on the body surface. By virtue of continuity of medium, a cavity formed behind the base is filing to Crocco's theorem

$$\vec{V} \times \vec{\omega} = - T \cdot \mathrm{grad}\, S,$$

the shocks with curved fronts (with entropy S varying along the front) represent the physical source of vorticity $\vec{\omega} = \mathrm{rot}\, \vec{V}$. This is the case of bow shock waves at $M_\infty > 1$ and internal shocks in the presence of local supersonic regions in flow.

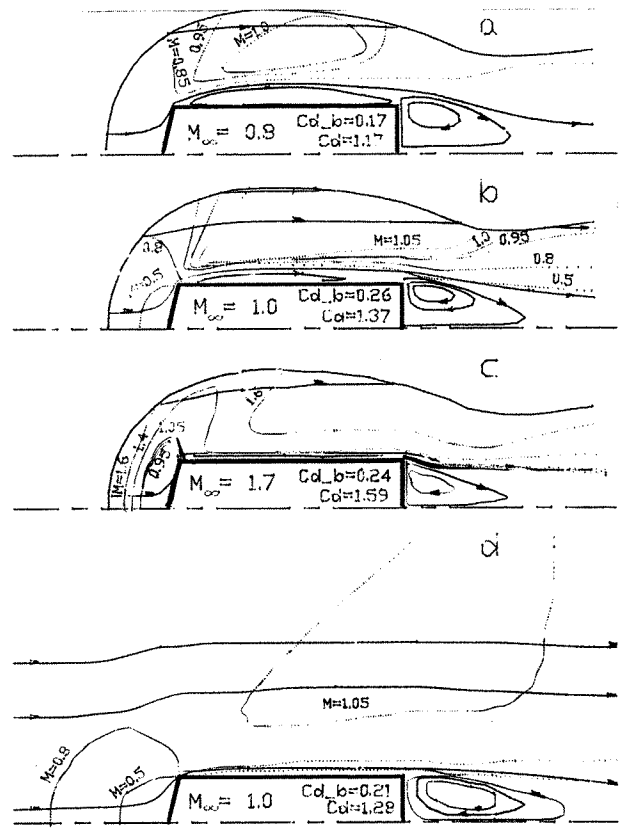

Figure 2. Computational results for the isolated reentry vehicle on the O (a,b,c) and H (d) grids.

The results of computation on the O-grid with skewed cells near the axis of symmetry (see Fig.1,b) at Mach numbers M_∞ = 0.8; 1.0; 1.7 and on the H-grid at M_∞= 1.0 are presented in Fig.2. Along with the body semicontour, depicted in this figure are the base drag coefficient C_{d_b} and the total drag coefficient C_d. The total drag coefficient increases monotonically, and the influence region is reorganized from elliptical into

h-yperbolical.

At $M_\infty = 0.8$ (Fig.2,a) the only source of vorticity is artificial viscosity. Along with a separated zone in the base region a long separated zone is observed on the cylindrical surface of the reentry vehicle aft of the cone-cylinder break. With increasing M_∞ and appearing physical vorticity in the flow the latter zone disappears, and the base separated zone loses its convexity, that is, the presence of negative (clockwise) vorticity in the flow make it easier for gas to flow past the cone-cylinder junction and the flat base, decreasing inertia of fluid particles and promoting the realization of the tangency conditions.

The computation on the H-grid (the semibody contour is approximated with 18 cells) presented in Fig.2,d gives a smaller extent of the separated zone on the cylindrical surface (which is explained by an additional vorticity introduced into the flow by the stepped line representing the cone) and a lower base drag.

The computation of flow around the isolated reentry vehicle at $M_\infty = 1.0$ was also conducted on the O-grid with orthogonal cells (Fig.1,c). The coefficients $C_{d_b} = 0.21$, $C_d = 1.33$ obtained as well as the shape of the Mach contours and the zeroth streamline in the base zone are closer to those predicted on the H-grid than the analogous results obtained on the O-grid with skewed cells. The distinctive feature of the last computation is the confluence of the separated zone on the cylindrical surface and the base separated zone through a narrow "neck". Later this grid was used for computing flow about the two-body system.

The schlieren photographs in Fig.3 were obtained in wind tunnel tests at Mach numbers $M_\infty = 0.86$ (Fig.3,a) and 1.1 (Fig.3,b). The Reynolds number based on the body diameter is about the same in both the cases and is equal to $Re_d = 0.5 \cdot 10^6$. As can be seen, the experiment also demonstrates weakening the separation on the cylindrical surface with increasing M_∞.

The computational results compare well with the experimental data on the base drag C_{d_b} (see, for example,[5]) and nose part drag $C_{d_n} = C_d - C_{d_b}$ from[11], where $C_{d_n} = 1.0$ was obtained at $M_\infty = 1$, $Re_d = 1.8 \cdot 10^6$.

Results of computing flow around the isolated parachute at a freestream Mach number of $M_\infty = 1.05$ presented in Fig.4 serve as the second example. The canopy shape was taken from photographs of models during wind tunnel tests at $Re_D = 3 \cdot 10^6$ and $M_\infty = 1.5$, the shape was assumed to vary little with decreasing M_∞. The computation was performed on two grids: O-type (Fig.4,a) and H-type (Fig.4,b). Along with the canopy shape, streamlines

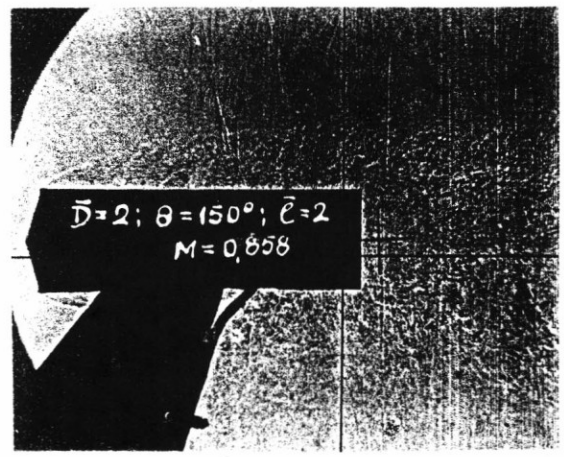

a

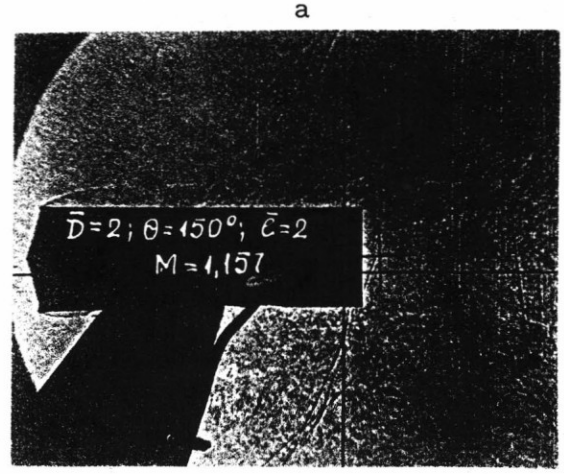

b

Figure 3. Experimental results for the isolated reentry vehicle.

and Mach contours, presented in this figure are the convergence time histories ($\bar{t} = \tau_0 \cdot I$) of the total drag coefficient C_D ($C_D \to 1.83$ on the first grid and $C_D \to 1.50$ on the second one) and the base drag coefficient C_{D_B} ($C_{D_B} \to 0.57$) computed on the first grid as well as

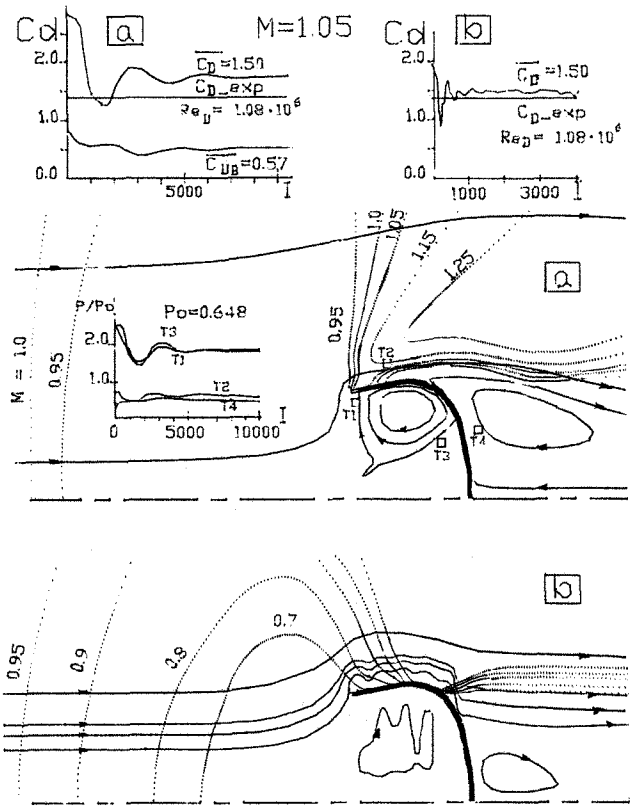

Figure 4. Computational results for the isolated parachute on the O (a) and H (b) grids.

values of the normalized pressure p/p_o for four points indicated in Fig.4,a: two points inside canopy (T1, T3) and two outside (T2,T4). As can be seen, the solution on the H-grid (the parachute semicontour is represented with 35 cells) converges faster: it takes only 1-2 thousand iterations whereas in the case of the O-grid with nearly the same number of grid points 5-10 thousand iterations are needed because of a smaller τ_o. In this case, the residual (averaged over the entire flowfield) for density

$$\Delta \rho = \frac{1}{I \cdot J} \sum_{i=1}^{I} \sum_{j=1}^{J} |\rho_{ij}^{N+1} - \rho_{ij}^{N}| / \tau_{ij}$$

diminishes by three orders of magnitude.

The isolated parachute introduces very large disturbances into flow, which reduces convergence rate by one order of magnitude as compared with reentry vehicle. In the case of the isolated reentry vehicle 100-200 iterations were sufficient at $M_\infty>1$ using the O-grid and up to 1000 at $M_\infty = 0.8$, with the nose part drag C_{d_n} converging nearly twice as fast as C_{d_b}.

The results obtained compare satisfactorily with experimental data and computational data from[2] on the drag coefficient of an isolated, impermeable, rigid parachute, where values of C_D=1.5-1.6 were found for a M_∞ range from 1.1 to 3.0. Some experiments reveal a monotonic increase in C_D from 1.3 to 1.45 as M_∞ increases from 0.6 to 0.9. The tests of an isolated rigid parachute of the same shape, carried out in the TsAGI T-112 wind tunnel at M_∞ =1.05-1.50 and Re_D= $1.1 \cdot 10^6$ to further verify the computational results, gave values of C_D = 1.33-1.43, with the drag maximum being at M_∞ = 1.15. These results agree well with the computation on the H-grid: the value of C_D is overpredicted by 2-9%. The agreement of the results on the O-grid is less satisfactory, they exceed an experimental value by 35-40%.

A better agreement of the computational results on the H-grid with the experimental value of C_D is explained by the fact that a sting support was used to mount the parachute in the wind tunnel, which decreased the size of the base separated zone and was not taken into account during computation. In computation on the H-grid this diminishing is attributed to additional vortex generation (and hence, to decreasing the cell Reynolds number) on the approximating stepped line. The additional vorticity in the internal vortex zone influences the solution in the external flow region through a Kutta-Joukowski-type condition on the sharp edge.

In both the experiment and computation the development of separation from the parachute sharp leading edge is observed, and with increasing M_∞ and generating additional (clockwise directed) vorticity on curved shocks the separated zone diminishes in height and is pressed to the canopy side surface.

Presented in Fig.5 are results of computing supersonic flow around the reentry vehicle-parachute configuration at $\overline{L}$ =L/D=1.75 and M_∞ =1.5. The ratio of the diameters of the reentry vehicle and parachute, D/d is equal to 6. The

presence of the forward body significantly changes the flow pattern. Fig.5a depicts computational results on the O-grid, and Fig.5,b on the H-grid. In this case, the flow around the two-body system has the so-called open wake pattern, where the reentry vehicle and parachute form a common separated zone beginning on the forward body and terminating behind the second body, so that the parachute drag (computed on the O-grid) $C_D = 0.58$ is substantially lower than at $L \to \infty$ and is primarily determined by the base drag $C_{D_B} = 0.43$. For comparison, the computation on the same grid for the isolated parachute gives $C_D = 1.76$, $C_{D_B} = 0.39$.

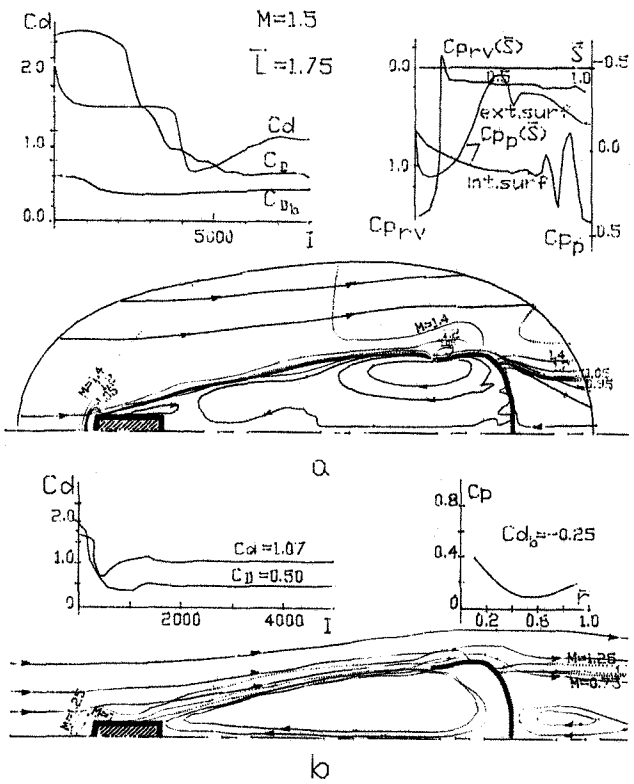

Figure 5. Computational results for the reentry vehicle-parachute configuration on the O (a) and H (b) grids.

The reentry vehicle's base drag is negative in this case: $C_{d_b}=-0.21$; there is an excessive pressure $C_p=(p-p_\infty)/q_\infty>0$. The nose part drag $C_{d_n} = 1.33$ varies little owing to the presence of the parachute. For the isolated reentry vehicle the computation on the same grid at $M_\infty = 1.5$ gives $C_{d_b}=0.25$, the mean value of the base pressure $\overline{C_{p_b}}=-0.25$, $C_{d_n} = 1.31$, that is, C_{d_n} for the reentry vehicle in the presence of the parachute practically does not vary, but the base drag varies significantly up to the sign change with parachute's approaching to the reentry vehicle, which is determined by the change-over of the flow pattern from the closed wake pattern, where an independent separated zone forms behind the reentry vehicle as in the case of the isolated vehicle, to the open wake pattern as in this case, where $C_{d_b}< 0$ is realized because of a common internal separated zone.

Presented in Fig.5,a are streamlines marked by arrows and contours M = const as well as the semicontours of the reentry vehicle and parachute and pressure distributions $C_p(\overline{s})$ along them, where $0\le \overline{s} \le 1$ is the arc length. The convergence histories of the reentry vehicle's total drag, the base drag C_{D_B}, and the total drag C_D of the parachute are also presented. As can be seen, the convergence takes 7 - 8 thousand iterations ($\overline{t}$ = 9 - 10).

A similar computation on the H-grid (see Fig.5,b) for the same flow pattern with open wake gives a smaller size of the separated zone behind the parachute and a somewhat smaller value of its total drag (this explains better agreement with the experiment, where the parachute was mounted on a sting support decreasing the base drag), $C_D= 0.50$. The values of the reentry vehicle's total and base drag coefficients, $C_d= 1.07$ and $C_{d_b}=-0.25$, respectively, also correlate well with the results obtained on the O-grid, but the solution stabilization in the last case is reached much faster, in N=1000 ($\overline{t}$=10). The pressure distribution over the reentry vehicle's base area $C_p(\overline{r})$ in Fig.5,b corresponds to $\overline{s}$=0.85-1.0 in the plot $C_{prv}(\overline{s})$ in Fig.5,a.

The calculations on both grids correlate well for C_d and C_D and also are in good agreement with experimental results for a soft parachute (mounted on suspension lines behind a reentry vehicle model), obtained in the TsAGI T-109 wind tunnel at $Re_D = 3\cdot10^6$, $M_\infty = 1.5$. A close agreement of the results on both the grids is observed for C_d at

M_∞=1.3 and for C_D at M_∞ =1.0. For other M_∞ values the computation on the O-grid gives a somewhat greater values of drag. It seems likely to be attributed to the differences in the parachute shapes in experiment and in calculation.

Tests in the T-109 wind tunnel on a rigid parachute at D/d = 4.6 (that is, smaller than in computation) give an appreciably larger value of C_D= 0.92 at M_∞ = 1.5. At smaller M_∞ the value of C_D obtained from the experiment is between the computed results for the O- and H-grids. At M_∞ = 1 they differ by no more than 10%. To better match the experimental data and the results computed on the O-grid the computational scheme must account for the presence of a sting support.

Comparison with wind tunnel testing shows that the computation reproduces physical features of flow well: a computed separation from the cone-cylinder juncture revealed by computation can be observed in experiment using visualization. Introduction of an additional vorticity into the flow by the first body (including nonphysical vorticity in computation) diminishes the drag of the parachute. The same is observed in tests where C_D for the sharp-nosed reentry vehicle (φ=22°) is larger than in the case of blunt-nosed one (φ=150°) at all values of M_∞ and L excluding small L = (2-3)·d at supersonic speeds ($M_\infty \geq 1.1$), when the sharp-nosed vehicle introduces a greater vorticity in flow enlarging the vehicle's wake due to λ-shocks on its cylindrical surface and ensuing separations.

Computations of the flow around the two-body system at lower freestream Mach numbers, performed on the O-grid, show unsteady quasiperiodical character of the flow when in the solution alongside the short-period oscillations with nondimensional period $\overline{T} = T \cdot V_\infty/D = 0.2$ there are long-period oscillation. For example, at M_∞ = 1.0 the total drag is periodical with a period of $\overline{T} = \Delta N \cdot \tau_0$ = 3.4 and an amplitude from min C_D = 0.50 to max C_D=1.30, the base drag C_{D_B} being nearly constant, which is associated with pulsations of the internal separated zone. In this case the reentry vehicle's total drag features short-period small-amplitude variations modulated by a long-period large-amplitude one. The same feature is characteristic of the time dependences of the pressure p/p_0 in the base zone and especially inside the parachute canopy, its oscillation, both short- and long-period, being in antiphase. On the nose part of the reentry vehicle and in the base zone of the parachute the pressure is nearly constant.

As in [4], where an unsteady solution of sonic flow around a sphere is presented, oscillations of the parameters investigated occur approximately at the same instants of time and does not depend on grid density and variation of the time step τ_0. In comparison with test data and steadystate solutions obtained on the H-grid, the drag values averaged over the slow oscillation period are used.

Long-period motion is connected with dividing and joining the regions of flow separation on the cone-cylinder junction and on the base and with "breathing" of the internal separated zone, the minimum C_D being observed when the internal separated zone is "inflated" and the maximum when it is "deflated". In this case the parachute canopy at a fixed distance plays a role of resonator and the oscillation period varies as a function of the freestream velocity and the distance between the bodies: thus, at $\overline{L}$ = 1 it is smaller than at $\overline{L}$ = 1.75, and $\overline{T}$ = 3.3 at M_∞ = 1.0.

The latter results are of interest because they demonstrate the possibility of obtaining an unsteady quasiperiodic solution in the framework of a stationary statement of the boundary-value problem but using an unsteady algorithm. Unsteadiness in the solution can occur also from decreasing the freestream Mach number M_∞ (as at $\overline{L}$ =1.75) and from diminishing the distance between the bodies: for example, solutions at $\overline{L}$ = 1 for all velocities in a range of $0.8 \leq M_\infty \leq 1.7$ is inherently unsteady.

There are two causes of difference between solutions for the same algorithm on two different grids with the same number of grid points. The first cause is a topological difference between the O- and H-grids and associated levels of solution approximation. Thus, unsteady solutions occur on the O-grid

because of smaller artificial viscosity. Unsteadiness manifests itself in the form of interactions of the separations on the side surface with the base separation. The second cause is scheme independent and introduced into the problem "from the outside". On the O-grid the smooth parts of bodies' surfaces approximated without steps, hence this grid better corresponds to a boundary-value problem. In the case of the H-grid, the stepped approximation for curved parts of the surfaces and the parts which do not coincide with the grid lines results in an additional vorticity generation at step corners, which diminishes the separated zone behind the parachute and hence the base drag. The presence of the sting support gives the same effect, which explains a better agreement between experiment and computation on the H-grid.

Good qualitative agreement between experimental and computational flow-field patterns and satisfactory agreement of computed results and force test data advocate the possible use of this approach in analysis of separated flows.

The authors would like to thank Dr. A.G.Ereza and Dr. V.S.Markin for kindly providing results of experimental studies.

References

1. Guvernyuk, S.V., Lokhansky, Ya.K., Savinov K.G. On a Numerical Investigation of the Aerodynamics of Thin-Walled Permeable Screens. Parachutes and permeable bodies, MGU Publisher, Moscow, 1987 (in Russian).

2. Baksheyev, S.P. Unsteady Aeroelastic Model of Permeable Axisymmetric Parachute Deployment in the Flow of Compressible Perfect Gas. KIIGA, Kiev, 1988 (in Russian).

3. Courant,R., Friedrichs,K.O., Lewy,H. Über die partiellen Differenzengleichungen der mathematischen Physik. Math. Annalen, Bd. 100, 1928.

4. Vyshinsky, V.V., Kravchenko,S.A. The Calculation of Separated Axisymmetric Flows over Bodies Based on the Euler Equation Solution in the Internal Fortex Region. Trudy TsAGI, issue 2494, 1990 (in Russian).

5. Vyshinsky, V. V., Kravchenko, S. A. 3-D Separated Flows by Euler Equations. TsAGI J., No 2, 1994.

6. Belotserkovskii,O.M., Davydov, Yu.M. Numerical Approach for Investigating Some Transonic Flow. Lect. Notes in Phys., Springer-Verlag, 19, p. 25 - 32, 1973.

7. Potter, D. Computational Physics. John Wiley & Sons Ltd., London-New York -Sydney-Toronto, 1973.

8. Belotserkovskii, O.M., Davydov,Yu.M. Numerical experiments for supersonic and hypersonic flows.Acta Astronautica, 1, No 11-12, p. 1467-1474, 1974.

9. Vyshinsky,V.V., Kravchenko,S.A., Sorokin, A.M. On the grid selection in solving aerodynamic problems. Voprosy Atomnoi Nauki i Techniki. Ser. Mathematical Modeling of Physical Processes, No 1, 1994 (in Russian).

10. Thomas, J.L., Salas, M.D. Far-field boundary conditions for transonic lifting solutions to the Euler equations. AIAA Paper 85-0020.

11. Petrov, K.P. Aerodynamics of vehicle's elements. Moscow, Mashinostroenie Publisher, 1985 (in Russian).